Published in final edited form as:
J Mol Biol. 2011 July 8; 410(2): 294–306. doi:10.1016/j.jmb.2011.05.015.

A Two Site Mechanism for the Inhibition of IAPP Amyloidogenesis by Zinc

Samer Salamekh[†], **Jeffrey R. Brender**[†,‡], **Suk-Joon Hyung**[†], **Ravi Prakash Reddy Nanga**[†], **Subramanian Vivekanandan**[†,‡], **Brandon T. Ruotolo**[†], and **Ayyalusamy Ramamoorthy**[†,‡,*]

[†] Department of Chemistry, University of Michigan, Ann Arbor, Michigan 48109-1055

[‡] Department of Biophysics, University of Michigan, Ann Arbor, Michigan 48109-1055

Abstract

Human Islet Amyloid Polypeptide (hIAPP) is a highly amyloidogenic protein cosecreted with insulin in response to glucose levels. The formation of hIAPP amyloid plaques near islet cells has been linked to the death of insulin-secreting beta-cells in humans and the progression of type II diabetes. Since both healthy individuals and those with type II diabetes produce and secrete hIAPP, it is reasonable to look for factors involved in storing hIAPP and preventing amyloidosis. We have previously shown that zinc inhibits the formation of insoluble amyloid plaques of hIAPP; however, there remains significant ambiguity in the underlying mechanisms. In this study, we show zinc binds unaggregated hIAPP at micromolar concentrations similar to those found in the extracellular environment. By contrast, the fibrillar amyloid form of hIAPP has low affinity for zinc. The binding stoichiometry obtained from ITC experiments indicates zinc favors the formation of hIAPP hexamers. High-resolution NMR structures of hIAPP bound to zinc reveal changes in the electron environment along residues that would be located along one face of the amphipathic hIAPP alpha-helix proposed as an intermediate for amyloid formation. Results from ESI-MS investigations showed that a single zinc is predominantly bound to hIAPP and revealed that zinc inhibits the formation of the dimer. At higher concentrations of zinc a second zinc binds to hIAPP, suggesting the presence of a low affinity secondary binding site. Combined, these results suggest zinc promotes the formation of oligomers while creating a energetic barrier for the formation of amyloid fibers.

Keywords

amylin; amyloid; metal-binding; structure

Introduction

Islet amyloid polypeptide, IAPP1 (sequence shown in Figure 1), is a 37 residue amyloidogenic peptide hormone secreted primarily by pancreatic β-cells in the islets of

*Corresponding Author: Ayyalusamy Ramamoorthy, ramamoor@umich.edu, Phone: 734-647-6572, Fax: 734-764-3323.

[1]Abbreviations: IAPP: Islet Amyloid Polypeptide, hIAPP: human Islet Amyloid Polypeptide, rIAPP: rat Islet Amyloid Polypeptide Aβ: amyloid Beta, ESI-MS: Electrospray Ionization Mass Spectroscopy, ITC: Isothermal Titration Calorimetry, TFE: trifluoroethanol, DMSO: Dimethyl sulfoxide

Langerhans in response to high glucose levels.[1] IAPP is cosecreted with insulin and has been shown to enhance the effects of insulin by slowing gastric emptying, reducing the rate of glucose entering the blood, and signaling the brain to reduce meal size.[1] However, human IAPP has a strong amyloidogenic propensity that has been linked to β-cell death in type II diabetics and in transgenic mice overexpressing the human IAPP variant.[2–6] The insoluble plaques are rich in β-sheet character, similar to those found in Alzheimer's, Parkinson's, Huntington's, Prion's disease, and other degenerative diseases.[7] While hIAPP can aggregate *in vitro* at low micromolar concentrations[8], the peptide is stored at millimolar concentration *in vivo*.[9–11] The kinetics of fibrillization and fiber morphology are highly dependent on conditions at which fibrillization takes place.[12] Since diabetics and non-diabetics have the same IAPP sequences, the cellular environment must contain factors that either accelerate aggregation or act as chaperones to stabilize the protein at the high concentrations.[13–20]

The dysregulation of metal ions in amyloid-related diseases has received particular attention following the discovery of a high prevalence of metal ions in amyloid deposits. It has been shown that amyloidogenic proteins, such as Aβ, α-synuclein, and mammalian prion protein, have transition metal binding sites that affect aggregation rates.[21–24] Although amyloid proteins are characterized by similar fiber structure and nucleation-dependent kinetics, the effect of metal ions on aggregation is highly dependent on the particular protein and metal.[7] For example, while copper has been shown to promote the formation of Aβ fibers, copper inhibits the formation of IAPP fibers.[25; 26] The role of zinc in type II diabetes and hIAPP aggregation is less understood as both zinc supplements and zinc chelation have been shown to decrease β-cell death and symptoms of type II diabetes. [27–29] These studies suggest zinc has a variety of effects on β-cells and stress the need for further investigation.

Zinc as a chaperone in regulating hIAPP fiber growth is of particular interest as the zinc content of β-cell secretory granules, where hIAPP is stored, is among the highest in the body and the pancreas is particularly sensitive to systemic zinc levels.[30] Although the molecular interaction of zinc to other amyloidogenic proteins, such as Aβ and mammalian prion protein has been characterized, little is known about how zinc interacts with hIAPP.[31–33] Zinc has already been shown to impact a variety of processes involved in glucose homeostasis, including storage and excretion of insulin, glucose-stimulated secretion cascades, and paracrine communication with α-cells; however, little is known about zinc's effect on IAPP-induced β-cell death.[34–36] Previous studies have shown that zinc accelerates the formation of fibers at pH 3; however, our recent investigation has shown that zinc has a bimodal effect on the aggregation rate of hIAPP at neutral pH.[37] The complex effects of zinc on hIAPP emphasize the need for a more comprehensive study of the molecular basis of the interaction.

In this study, we attempt to further characterize the nature of zinc binding to hIAPP using isothermal titration calorimetry, dye binding assays, electrospray ionization mass spectrometry (ESI-MS), and NMR. We show that zinc binds to monomeric IAPP near the His 18 residue with low micromolar affinity. The affinity of the fibrillar hIAPP for zinc is significantly less than the monomeric form. We also show that zinc is displaced from monomeric IAPP during aggregation. ITC revealed that zinc preferentially binds 6 hIAPP monomers in a conformationally–dependent manner. Concurrently, ESI-MS revealed the formation of the dimer is inhibited by the presence of zinc. High-resolution NMR structures of hIAPP in the presence and absence of zinc reveal long-range structural variations in the amphipathic region of the previously proposed α-helix conformation of the dimer. The results indicate that zinc inhibits fibrillization by creating a thermodynamic barrier for the formation of mature fiber and dimer, while promoting the formation of oligomers.

Results

Human IAPP binds zinc with low micromolar affinity

We previously showed that zinc has an overall inhibitory effect on fibril formation while having a concentration-dependent bimodal effect on hIAPP fibrillogenesis.[37] At low concentrations, zinc increases the lag-time for fiber formation and decreases the rate of addition of hIAPP to existing fibers, while the effect begins to reverse at higher concentrations. To understand the molecular origin of the inhibitory effect, we first attempted to quantify the binding affinity of hIAPP initially prepared in the monomeric state to $ZnCl_2$ by isothermal titration calorimetry (ITC). However, the rapid aggregation of hIAPP in solution proved to be problematic for the accurate determination of binding constants, as aggregation during titration can cause both an enthalpy change associated with IAPP self-association in addition to a change in the types of oligomeric species present.[38] Since each oligomer may have differing affinities for the metal ion, oligomerization of IAPP can severely complicate analysis. To overcome this problem, a fragment of hIAPP ($hIAPP_{1–19}$) was chosen that retains the residues implicated in metal ion binding but does not form fibrils on the timescale of the experiment. [37; 39–42]

Zinc chloride was initially titrated into $hIAPP_{1–19}$ in a low ionic strength buffer (100 mM Tris, 100 μM NaCl, pH 7.3) to maximize the enthalpy evolved upon zinc binding. A single binding site was observed at a substoichiometric ratio of 0.14 zinc : peptide (see Figure 2). The approximately six to one stoichiometry indicates octahedral coordination of hIAPP to zinc, without coordination of water to solvent in the IAPP-zinc complex. Zinc bound $hIAPP_{1–19}$ with comparatively high affinity ($K_{d,app}$ 1.12 μM) and a ΔH of −61.9 kJ/mole, corresponding to a ΔS of −93.8 J/mol. To investigate the zinc binding affinity at a more physiologically-relevant salt concentration, a high ionic strength buffer (100 mM Tris, 100 mM NaCl, pH 7.3) was used. A similar stoichiometry (0.15 zinc : peptide) and $K_{d,app}$ (1.23 μM) were observed. However, the apparent enthalpic contribution from the interaction is smaller in the high salt environment, with a ΔH of −25.6 kJ/mole, but the entropic contribution of the interaction is significantly higher with a ΔS of +27.2 J/mole.

The high affinity of zinc for $hIAPP_{1–19}$ is unusual, as hIAPP does not have a classic zinc-binding motif and only one residue (His18) that is considered a high affinity ligand for zinc. To test if the binding is specific for hIAPP, we performed a control titration with $ZnCl_2$ of MSI-361, an antimicrobial peptide of similar size containing a single histidine like $hIAPP_{1–19}$ and hIAPP (sequence shown in Figure 1). Binding of zinc to MSI-361 was not detected at the concentrations used in the experiment (Figure 3), suggesting binding of zinc to hIAPP is sequence-specific. Zinc also did not bind to the rat version of IAPP (Figure 3, sequence in Figure 1) which has a His18Arg substitution, confirming the importance of this residue in binding.

To determine the effect of secondary structure on the binding of zinc to $hIAPP_{1–19}$, ITC experiments were repeated in the presence of 30% 2,2,2-trifluoroethanol (TFE), a solvent that causes hIAPP to favor the α-helix conformation.[43; 44] While zinc binds to the primary binding site with comparable affinity, comparison of titration curves in the presence of TFE (Figure 4) reveals a shift towards a higher zinc : IAPP stoichiometry and the addition of an endothermic secondary binding site that was completely absent in the titration with Tris buffer only. The parameters suggest the α-helical conformation of the peptide has steric constraints when bound to zinc. This is likely the result of increased crowding around the zinc center caused by the bulky helical structure as compared to the random coil structure in solution. Although there is a shift in stoichiometry, the small increase in apparent dissociation constant suggests that the additional hIAPP monomers bound to zinc in the

absence of TFE either cause existing zinc-IAPP interactions to weaken or the additional monomers are minor contributors to the thermodynamics of binding.

Zinc dissociates from hIAPP$_{1–37}$ during fiber formation

The ITC experiments showed freshly dissolved hIAPP$_{1–19}$ has a relatively high affinity for zinc in the context of the very high zinc concentrations present in the secretory granule. Unfortunately, enthalpy changes occurring from mechanical breakage of fibers during stirring prevent the accurate measurement of zinc binding to the fibrillar form of hIAPP. Instead, a dye displacement assay was used, using the displacement of zinc from hIAPP as a function of the concentration of the zinc-binding dye Fluozin-1 to determine the approximate relative affinity of zinc for hIAPP in the monomeric and fibrillar states. The Fluozin-1 dye is fluorescent when bound to zinc and essentially non-fluorescent when not, allowing a measurement of the relative affinity of zinc for different aggregation states.

To determine if zinc is displaced from the monomeric hIAPP$_{1–37}$ during fiber formation, the peptide was added to a solution of the fluorescent zinc sensor FluoZin-1 along with zinc and allowed to fibrilize. Fluozin-1 was first titrated with hIAPP$_{1–37}$ freshly dissolved in DMSO at 4°C. At this temperature, hIAPP$_{1–37}$ does not aggregate, allowing measurement of hIAPP$_{1–37}$ in the soluble state. Addition of peptide up to 6 μM causes a decrease the fluorescence signal, indicating the peptide is binding to zinc and displacing it from the Fluozin-1 (Figure 5). At 6 μM the temperature was raised to 25°C and titration of the peptide in DMSO continued. At 8 μM titration was stopped and the solution allowed to stand until it became visibly cloudy. A large increase in the fluorescence intensity was observed at this point, corresponding to the zinc being displaced from the peptide during fiber formation and rebinding to the zinc sensor (Figure 5). Further addition of monomeric hIAPP$_{1–37}$ results in a decrease of fluorescence intensity due to zinc being displaced from Fluozin-1 by the addition of freshly added peptide.

ESI-MS indicates Zn^{+2} disrupts dimer formation

Since the stoichiometry of binding suggests several monomers interact with a single zinc, we investigated further the possibility that zinc promotes the formation of hIAPP$_{1–37}$ oligomers. To determine the effect of zinc on the oligomeric state of hIAPP$_{1–37}$, we employed ESI-MS using a nanoflow ESI source and gentle dessolvation to retain native non-covalent contacts. Only the monomeric state of hIAPP$_{1–37}$ and small oligomers are observable by ESI-MS, as amyloid fibers and large oligomers with a very high molecular mass are not efficiently ionized. Consequently, the distribution of oligomers obtained by ESI-MS may not reflect the true distribution of oligomers existing in solution.

In the absence of zinc, a single major peak is observed at 1952 m/z (Figure 6A). This value corresponds to a hIAPP$_{1–37}$ monomer in the +2 charge state, indicating the majority of the ionized peptide is in the monomeric state. However, a minor peak is observed at 2604 m/z that corresponds exactly to the expected mass of a hIAPP$_{1–37}$ dimer in the +3 charge state. Interestingly, the peak at 2604 m/z corresponding to the native dimer is not observed in the presence of zinc. The loss of the dimer peak with the addition of zinc indicates that zinc disrupts the formation of dimers that are formed in the absence of metal. Larger oligomer species were not observed, either because their non-covalent interactions are weaker than dimers or they were not ionized efficiently under the MS-compatible solution condition employed.

The ESI-MS data confirms that hIAPP$_{1–37}$ binds 1 zinc atom in the presence of a high excess of $ZnCl_2$, as shown by an intense peak at 1984 m/z seen in the presence 1 mM $ZnCl_2$ (Figure 6C). In addition, a smaller population of hIAPP$_{1–37}$ bound to 2 zinc atoms is also

indicated by the peak at 2016 m/z. The origin of the second binding site is uncertain, but a possible binding site exists if the disulfide bond is broken during the ionization process. To rule out this possibility, the ESI-MS experiment was performed with reduced $hIAPP_{1–37}$. The large increase of zinc-bound $hIAPP_{1–37}$ compared to the oxidized peptide (Figure 6C, D) suggests the disulfide bond is intact and Cys2-Cys7 is not the source of the second binding site.

To examine the strength of the second binding site in more detail, a titration of 10 μM $hIAPP_{1–37}$ was performed from 1–5000 μM $ZnCl_2$. The titration showed a high affinity binding site that saturates at 10 μM $ZnCl_2$ (Figure 7 inset). In addition, a second binding weak affinity site becomes evident at millimolar concentrations of zinc (Figure 7A). The data could be fit to a two site independent binding model with K_d values of ~2 μM and ~1200 μM (Figure 7B), in agreement with the 1.1 μM value obtained by ITC for $hIAPP_{1–19}$ (Table 1). A fraction of the peptide remained unbound even at saturating concentrations of zinc, most likely reflecting dissociation of zinc during the ionization process. However, the existence of soluble and ionizable species of hIAPP unable to bind zinc cannot be excluded. In summary, the ESI-MS data shows soluble $hIAPP_{1–37}$ is exclusively bound to one zinc at low (micromolar) concentrations of zinc, while at higher (millimolar) zinc concentrations a substantial fraction of the population binds to two zinc atoms.

Binding of zinc induces localized changes near His 18 and long-range effects on the N-terminus region involved in self-association

To understand the structural changes that occur in hIAPP upon zinc binding, we have examined perturbations of the electronic environment accompanying the binding of $hIAPP_{1–37}$ to zinc and solved the high-resolution structures of $hIAPP_{1–19}$ in the absence and presence of zinc. Previously, we solved the high-resolution NMR structure of hIAPP bound to zinc in 22% HFIP, 8% TFE.[37] This organic solvent solution strongly promotes α-helix formation, which is a minor conformer believed to be a structural intermediate in the fibrillogenesis pathway. The observation that low concentrations of helix-promoting organic solvents accelerate hIAPP fibril formation provides strong evidence that the α-helix conformer is a structural intermediate in dynamic conformational equilibrium with the unstructured conformer.[45] To examine structural perturbations caused by zinc binding in the aqueous state, we acquired SOFAST-HMQC spectra of recombinant ^{15}N labeled $hIAPP_{1–37}$ in the absence and presence of 1 mM $ZnCl_2$ at pH 5.5. Amidation of the C-terminus is known to increase the rate of fibrillization,[46] but its impact on zinc binding and on the formation of smaller oligomeric species is unknown. The SOFAST technique was used to speed up data acquisition and minimize the peptide aggregation during the course of the NMR experiment that may cause artifacts as noted above. Using this technique, the acquisition time was reduced from the 60 minutes required to obtain a conventional spectra to approximately 6 minutes, a brief enough time-period that no changes were noted in successive scans in the absence of zinc.

An overlay of the 2D ^{15}N-^{1}H SOFAST-HMQC spectra in the absence (red) and presence (blue) of zinc is presented in Figure 8. All of the residues could be unambiguously identified with the exception of the first two N-terminal residues and Gln 10. As expected, the most significant changes in chemical shift upon zinc binding are centered near His 18, indicating coordination to zinc at that site. In addition, smaller chemical shift changes can also be detected in two distinct regions of the peptide, the first centered at the N-terminal region and the second at the disulfide bridge region from Asn 3-Ala 8.

The existence of chemical shift changes distal to the zinc-binding site in the predominantly unstructured hIAPP peptide indicates zinc-binding induces changes beyond the local structural distortions at the zinc binding site. The N-terminal region is implicated in both

hIAPP self-association[47–49] and in the hIAPP helix-coil transition,[46; 50] while the disulfide bridge region is highly sensitive to environmental effects. These changes are therefore consistent with either an alteration in the helix to coil conformational equilibrium or alterations in self-association interactions. To examine changes in this region in more detail, we solved the high-resolution structures of $hIAPP_{1–19}$ in a highly helical state using 30% TFE in the absence and presence of zinc. An overlay of the 2D ^{1}H-^{1}H TOCSY spectra of $hIAPP_{1–19}$ (Figure 9) in the absence (red) and presence (blue) of zinc shows noticeable downfield changes in the H_N chemical shifts along one side of the amphipathic helix at Cys7, Gln10, Ala 13, Leu 16 in addition to upfield changes for Thr 9 and Arg 11 (see Figure 10). The N-terminus becomes more ordered upon the binding of zinc (Figure 11), a change reflected in the increased number of NOEs within this region. Overall, the pattern of chemical shift changes for $hIAPP_{1–19}$ in the helical state is consistent with that of the SOFAST experiment of $hIAPP_{1–37}$ in the aqueous state at pH 5.5.

Discussion

Our previous studies have shown that zinc has a complex effect on amyloid formation by hIAPP. [37] While zinc decreases the amount of hIAPP fibers formed, the final fibers formed are similar to those formed in the absence of zinc, in contrast to most other inhibitors in which the fibers are noticeably shorter or display other signs of aberrant morphology. Similarly, zinc has a complex effect on the kinetics of amyloid formation. At low concentrations, zinc inhibits IAPP amyloid formation, decreasing both the elongation time and the lag-time for amyloid formation, while at higher concentrations the effect begins to reverse itself. Finally, zinc has an opposite effect at a low pH similar to that found in the secretory granule, as elongation rates increase and lag times decrease in a nearly linear fashion with the addition of zinc.

The displacement of zinc precedes the formation of mature fiber

To explain these apparently contradictory findings we first measured the affinity of zinc for hIAPP in the monomeric and fibrillar state. Using the fluorescent indicator FluoZin-1, we showed that zinc binds to amyloid fibers with significantly decreased affinity compared to the monomeric peptide and is displaced upon fibrillization (Figure 5). In the fiber form, His18 is located in the turns of the anti-parallel β-sheet structure where previous studies have shown the charge of the residue has a large effect on the rate of fibrillization.[51; 52] Incorporation of a charged species into the fiber would therefore result in electrostatic repulsion between adjacent β-sheet strands that would propagate into the fiber morphology and be visible by EM, TEM, or AFM.[53] Our results indicate that zinc is not incorporated into the fiber and must be displaced prior to the formation of the mature fiber, increasing the thermodynamic barrier for amyloid formation.

However, kinetic assays of fiber formation indicate millimolar concentrations of zinc start to accelerate fiber formation. The ESI-MS data indicates acceleration of fiber formation may be due to the binding of zinc at a second low-affinity binding site. At low concentrations of $ZnCl_2$, only a single Zn is bound to the peptide. However, at higher concentrations of $ZnCl_2$, a substantial fraction of the peptide is bound to 2 Zn ions (Figure 7), indicating the presence of a second binding site with millimolar affinity. The existence of two-binding sites, one high and one low affinity, correlates with the kinetic data that shows that zinc inhibits fiber formation at low concentrations but the degree of inhibition significantly decreases at millimolar concentrations. After saturation of the high-affinity, inhibitory, binding site the second low-affinity binding site becomes occupied, which accelerates fiber formation (see Figure 12 for a cartoon depiction).

hIAPP binds to zinc as a hexamer by minimizing unfavorable steric interactions

Somewhat surprisingly, the ITC experiments showed that zinc binds to hIAPP with low micromolar affinity. This finding was surprising in that it is difficult to predict the strong apparent affinity based on the hIAPP peptide sequence alone as the peptide contains only one residue (His 18) that binds zinc tightly. Individually, the imidazole of histidine has a binding constant for zinc in the low millimolar range, which is significantly higher than the low micromolar binding that our studies revealed.[54; 55] A minimum of 3 histidines are required to obtain the low micromolar apparent binding affinity observed for hIAPP, assuming no additional unfavorable process such as steric hindrance takes place. Given that zinc prefers to bind 4–6 ligands,[31] the high apparent binding affinity suggests several hIAPP molecules are coordinated with a single zinc. The substoichiometric ratios of binding found from the ITC measurements correlate to a complex of approximately 1 zinc to 6 hIAPP molecules. A 6 ligand zinc complex is larger than typically found in proteins that interact with zinc; however, the relatively unstructured nature of hIAPP may facilitate additional bound ligands.[56; 57] A 4 ligand zinc complex was indicated for the $hIAPP_{1–19}$ peptide in the helical state, suggesting that conformational flexibility may play a role in reducing steric crowding. Conformational flexibility likely plays a larger role in the binding of zinc to the full-length peptide. Previously reported high-resolution structures of $hIAPP_{1–37}$ in the α-helical conformation revealed a zinc-induced kink in the α-helix near His 18 that could serve to minimize unfavorable steric interactions as the monomers attempt to coordinate around zinc.[37] It is uncertain to what degree conformational flexibility affects zinc binding; however, the similar binding affinity of $hIAPP_{1–19}$ in the two states suggests the energetic difference between tetrahedral and octahedral coordination is minimal for $hIAPP_{1–19}$.

Zinc inhibits the formation of the hIAPP dimer and mature fiber while promoting the formation of oligomers

ITC results and our previous results suggest that zinc promotes hIAPP oligomerization, but amyloid formation is complex and frequently involves a variety of on- and off-pathway oligomeric intermediates. In the absence of zinc, ESI-MS detected a peak corresponding exactly to the expected molecular weight of dimeric hIAPP. This peak was not apparent in the mass spectra of zinc-hIAPP, suggesting that, in addition to forming zinc bound oligomers, zinc suppresses the natural self-association of the peptide occurring in the absence of zinc.

The structure of this dimer is unknown, however, two basic models have been proposed for the initial steps of amyloid formation from natively unfolded peptides such as hIAPP. A variety of experimental and theoretical approaches have indicated that monomeric hIAPP is in conformational equilibrium between a largely random coil state, a partially helical state, and a β-hairpin conformation. In the first model, the amyloid fiber forms directly from the self-association of peptides in the β-hairpin conformation. The suppression of the dimer peak in the mass spectrum of zinc-bound IAPP is consistent with this model, as molecular dynamics simulations show the β-hairpin conformation has a similar structure as the subunits making up the final amyloid fiber.[58; 59] Further, dye competition assays showed preferential binding of zinc to the monomeric peptide compared to the amyloid form, and as a result the conformational equilibrium can be expected to shift away from the amyloid form.

In the second model, aggregation nucleates first from the association of partially α-helical conformers.[50; 60–63] In this model, the close proximity of the unstructured and aggregation prone regions of the peptide to each other drives the formation of β-sheet strands and conversion to the amyloid form. A high-resolution model for this type of association is provided by the crystal structure of IAPP fused to maltose binding protein, in which hIAPP

forms a helical dimer similar to the helix-turn-helix NMR structures observed for hIAPP in organic solvents and in detergent micelles.[64–66] Unlike some other natively unfolded amyloid proteins such as Aβ,[67; 68] helical intermediates have not been directly observed for hIAPP. However, substantial indirect evidence from a variety of sources supports the importance of the helical conformation, including the catalytic effect of trace amounts of helix-promoting solvents and the effect of inhibitors designed specifically to target the helical state.[62]

The crystal structure of dimeric hIAPP argues against the incorporation of zinc into a helical dimer.[64] In this structure, His 18 is rotated away from the dimeric interface, making a bridging interaction between hIAPP monomers involving His 18 unlikely. If zinc is bound to hIAPP in a conformation similar to the helical dimer observed in the crystal structure, we would expect to see the largest changes at the interface of the hydrophobic face of the helix at Leu 12 and Phe 15. By contrast, the strongest changes observed in our NMR experiments are away from the Zn binding site at Gln10, Ala13, and Leu16. While the (i, i+3) periodicity is consistent with zinc binding to a helical conformation (Figure 10), the distribution suggests association occurs at a different site along the helix.

Conclusion

In the present study, we have unraveled the underlying mechanism by which zinc affects fibril formation, self-association, and oligomerization. The strong affinity of freshly dissolved hIAPP for zinc and stoichiometry analysis has shown that several monomers coordinate around a zinc center, and in the process, off-pathway oligomers are stabilized. The suppression of dimers was further characterized by high-resolution NMR structures of the zinc-bound α-helical intermediates. Structural analysis revealed perturbations in the amphipathic region of hIAPP that has been repeatedly linked to self-association and bridging of dimers is an unlikely event. The weak affinity of the mature fibrils for zinc and previously reported models for aggregation pathways indicate the presence of zinc inhibits the formation of mature fibers and pushes the conformational equilibrium toward soluble oligomeric species.

Although the results of the study have begun to reveal the molecular basis by which zinc inhibits fiber formation, the complexity of the cellular environment must be taken into account when extrapolating the results to *in-vivo* events. The concentration of zinc localized around hIAPP in islet cells is neither static in time nor isolated from other cellular components. In its lifetime, IAPP experiences a broad range of conditions: from high millimolar concentrations of zinc in the presence of zinc-bound peptides, such as insulin, to picomolar concentration of extracellular zinc.[69] It is therefore not clear to what extent each of the mechanisms proposed affects hIAPP homeostasis when placed in the dynamic environment of the cell. Additional studies on the spatial and time-resolved cellular events related to hIAPP and zinc would increase our understanding of the cellular role of zinc in hIAPP homeostasis.

Materials and Methods

Peptide Preparation

Unlabeled human-$IAPP_{1–37}$ was purchased from SynBioSci (Livermore, CA), ^{15}N-labeled human-$IAPP_{1–37}$ was purchased from rPeptide (Bogart, GA), MSI-361 was obtained from Macromolecular Resources (Fort Collins, CO), rat-$IAPP_{1–37}$ was purchased from GenScript Corp (Piscataway, NJ), and unlabelled human-$IAPP_{1–19}$ was synthesized as previously described.[37] All IAPP peptides contain an oxidized disulfide between Cys 2 and Cys 7. Unlabelled peptides are amidated and the ^{15}N-labelled $hIAPP_{1–37}$ is unamidated. IAPP

samples were weighed out and dissolved in hexafluoroisopropanol (HFIP) to dissolve any small aggregates and lyophilized. Samples were rehydrated in corresponding buffer at 4°C immediately prior to use. To minimize zinc contamination, Milli-Q water was further purified on a cation exchange column with Chelex 100 (Bio-Rad, Richmond, CA). The concentration of $hIAPP_{1–19}$ peptide was determined using the peptide bond absorbance at 205 nm and a mean extinction coefficient of 32.5 ml/(mg × cm).[70; 71] $hIAPP_{1–37}$ fibers used in the study were grown with and without 2.5 μM zinc chloride for 10 days The presence of fibers was determined by turbidity measurements at 400 nm.

Isothermal Titration Calorimetry

ITC experiments were conducted at 25°C on the Nano ITC Standard volume calorimetry (TA Instruments, New Castle, DE). The samples were prepared with and without trifluoroethanol (TFE) such that the final concentration was 100 mM Tris buffer at pH 7.3 and either 100μM NaCl or 100 mM NaCl. Samples were degassed under vacuum for 15 minutes prior to being loaded into the ITC and stirred at 300 RPM. Control heat of dilution experiments were performed by titrating zinc chloride into buffer resulting in a negligible heat of dilution enthalpy (ΔH=−0.76 kJ/mol). ITC results were analyzed using the supplied Nano Analyze software (version 2.1.6), utilizing a one binding site model. ΔG values were calculated from the equilibrium constants (Eq. 1) and entropy values were determined from the Gibbs free energy equation (Eq. 2). The 95% confidence intervals for parameters directly determined by the ITC were calculated from the supplied software. The ΔS confidence interval was determined by standard propagation of error from the Gibbs free energy equation.

$$\Delta G = -RT\ln(K_d^{-1}) \quad (1)$$

$$\Delta G = \Delta H - T\Delta S \quad (2)$$

Competitive Dye Binding Assay

Displacement of zinc $hIAPP_{1–37}$ aggregation during was determined by competitive assay with the fluorescence zinc sensor, FluoZin-1 (Molecular Probes, Eugene, OR). The manufacturer determined K_d of FluoZin-1 for zinc is 8 μM with an excitation wavelength of 495 nm and emission wavelength of 515 nm. These values were verified under our conditions (10 mM Tris, 100 mM NaCl, pH 7.3) using excitation and emission bandwidths of 2 nm. Lyophillized $hIAPP_{1–37}$ was dissolved in DMSO to a concentration of 1 mM and then added to 2.5 μM FluoZin-1 and 2.5 μM $ZnCl_2$ in a 2 ml stirred cuvette. The experiment was initially performed at 4 °C to maintain the peptide in the soluble state. The temperature was then allowed to incubate at 25 °C to initiate fiber formation as described in the text.

Mass Spectrometry

Mass spectra of 25 μM hIAPP in 100 mM ammonium acetate buffer (pH 7.6) were obtained on a quadropole-ion mobility-time-of-flight mass spectrometer (Synapt HDMS G2, Waters, Milford MA, USA), according to a protocol described previously.[72] For assessing the binding stoichiometry of $hIAPP_{1–37}$ upon zinc binding, $ZnCl_2$ was added in excess, to a final concentration of 1 mM. Instrument parameters were optimized to retain non-covalent interactions in the peptide-zinc complex. The following instrument parameters were used: capillary voltage, 1.5 kV; sample cone 50 V; cone gas, off; ion transfer stage pressure, 4.40 mbar; trap pressure, 2.67×10^{-2} mbar; ion mobility cell pressure, 3.45 mbar; ToF analyzer

pressure, 1.39×10^{-6} mbar. All mass spectra were calibrated externally using an aqueous solution of cesium iodide (100 mg ml^{-1}) and were processed with MassLynx software (Version 4.1, Waters, Milford MA, USA). Spectra are shown with minimal smoothing and without background subtraction.

NMR Data Collection and Processing

All spectra were collected on a 900 MHz Bruker Avance NMR spectrometer equipped with a triple-resonance z-gradient cryogenic probe optimized for ^{1}H-detection.[73] SOFAST-HMQC spectra of 80 μM $hIAPP_{1–37}$ in solution (20 mM Tris, 50 mM NaCl, pH 5.5) were recorded at 4°C with 128 t_1 experiments, 4 scans, and a 100 ms recycle delay. Since $hIAPP_{1–19}$ is conformationally stable under the timescale of our experiments, NMR spectra of 1 mM $hIAPP_{1–19}$ in 30% deuterated TFE were obtained at 25°C and pH 7.5. Homonuclear experiments such as 2D ^{1}H-^{1}H TOCSY (Total Correlation Spectroscopy) and 2D ^{1}H-^{1}H NOESY (Nuclear Overhauser Enhancement Spectroscopy) were recorded at 80 and 300 ms mixing time, respectively in order to assist with backbone and sidechain assignments. The final 2D data matrix size was 2048 X 2048 after zero-filling in both dimensions. 2D data was processed using TOPSPIN 2.1 (from Bruker). Resonance assignment and volume fit calculations were performed using SPARKY 3.113.[74]

Structure Calculations

Final structures were calculated with the CYANA 2.1 program package using simulated annealing in combination with molecular dynamics in torsion angle space. NOE connectivities were used for the calculation of dihedral angle restraints. Unambiguous long-range NOE constraints were used during the first round of structure calculations to generate a low-resolution fold for the structure. The remaining ambiguous NOE cross-peaks were assigned in an iterative fashion by applying a structure-aided filtering strategy in repeated rounds of structure calculations. A total of 200 conformers were calculated in 8000 annealing steps each after complete assignment of resonances and the best 20 low energy conformers were selected and visualized using MOLMOL.

Acknowledgments

This study was supported by research funds from NIH (DK078885 and RR023597 to A.R.). We thank the 900 MHz NMR facility at the Michigan State University.

References

1. Woods SC, Lutz TA, Geary N, Langhans W. Pancreatic signals controlling food intake; insulin, glucagon and amylin. Philos Trans R Soc B. 2006; 361:1219–1235.
2. Leonardi O, Mints G, Hussain MA. Beta-cell apoptosis in the pathogenesis of human type 2 diabetes mellitus. Eur J Endocrinol. 2003; 149:99–102. [PubMed: 12887285]
3. Butler AE, Janson J, Bonner-Weir S, Ritzel R, Rizza RA, Butler PC. Beta-cell deficit and increased beta-cell apoptosis in humans with type 2 diabetes. Diabetes. 2003; 52:102–110. [PubMed: 12502499]
4. Dekoning EJP, Morris ER, Hofhuis FMA, Posthuma G, Hoppener JWM, Morris JF, Capel PJA, Clark A, Verbeek JS. Intracellular and extracellular amyloid fibrils are formed in cultured pancreatic-islets of transgenic mice expressing human islet amyloid polypeptide. Proc Natl Acad Sci U S A. 1994; 91:8467–8471. [PubMed: 8078905]
5. Haataja L, Gurlo T, Huang CJ, Butler PC. Islet amyloid in type 2 diabetes, and the toxic oligomer hypothesis. Endocr Rev. 2008; 29:303–316. [PubMed: 18314421]
6. Janson J, Ashley RH, Harrison D, McIntyre S, Butler PC. The mechanism of islet amyloid polypeptide toxicity is membrane disruption by intermediate-sized toxic amyloid particles. Diabetes. 1999; 48:491–498. [PubMed: 10078548]

7. Harrison RS, Sharpe PC, Singh Y, Fairlie DP. Amyloid peptides and proteins in review. Rev Physiol Biochem Pharmacol. 2007; 159:1–77. [PubMed: 17846922]
8. Ward B, Walker K, Exley C. Copper(II) inhibits the formation of amylin amyloid in vitro. J Inorg Biochem. 2008; 102:371–5. [PubMed: 18022240]
9. Nishi M, Sanke T, Nagamatsu S, Bell GI, Steiner DF. Islet amyloid polypeptide - a new beta-cell secretory product related to islet amyloid deposits. J Biol Chem. 1990; 265:4173–4176. [PubMed: 2407732]
10. Mirzabekov TA, Lin MC, Kagan BL. Pore formation by the cytotoxic islet amyloid peptide amylin. J Biol Chem. 1996; 271:1988–1992. [PubMed: 8567648]
11. Quist A, Doudevski L, Lin H, Azimova R, Ng D, Frangione B, Kagan B, Ghiso J, Lal R. Amyloid ion channels: A common structural link for protein-misfolding disease. Proc Natl Acad Sci U S A. 2005; 102:10427–10432. [PubMed: 16020533]
12. Goldsbury CS, Cooper GJS, Goldie KN, Muller SA, Saafi EL, Gruijters WTM, Misur MP. Polymorphic fibrillar assembly of human amylin. J Struct Biol. 1997; 119:17–27. [PubMed: 9216085]
13. Hoppener JWM, Ahren B, Lips CJM. Islet amyloid and type 2 diabetes mellitus. N Engl J Med. 2000; 343:411–419. [PubMed: 10933741]
14. Brender JR, Lee EL, Hartman K, Wong PT, Ramamoorthy A, Steel DG, Gafni A. Biphasic effects of insulin on islet amyloid polypeptide membrane disruption. Biophys J. 2011; 100:685–92. [PubMed: 21281583]
15. Knight JD, Williamson JA, Miranker AD. Interaction of membrane-bound islet amyloid polypeptide with soluble and crystalline insulin. Protein Sci. 2008; 17:1850–1856. [PubMed: 18765820]
16. Larson JL, Miranker AD. The mechanism of insulin action on islet amyloid polypeptide fiber formation. J Mol Biol. 2004; 335:221–231. [PubMed: 14659752]
17. Ma Z, Westermark GT. Effects of free fatty acid on polymerization of islet amyloid polypeptide (IAPP) in vitro and on amyloid fibril formation in cultivated isolated islets of transgenic mice overexpressing human IAPP. Mol Med. 2002; 8:863–868. [PubMed: 12606822]
18. Bedrood S, Jayasinghe S, Sieburth D, Chen M, Erbel S, Butler PC, Langen R, Ritzel RA. Annexin A5 directly interacts with amyloidogenic proteins and reduces their toxicity. Biochemistry. 2009; 48:10568–10576. [PubMed: 19810772]
19. Hull RL, Zraika S, Udayasankar J, Kisilevsky R, Szarek WA, Wight TN, Kahn SE. Inhibition of glycosaminoglycan synthesis and protein glycosylation with WAS-406 and azaserine result in reduced islet amyloid formation in vitro. Am J Physiol Cell Physiol. 2007; 293:C1586–93. [PubMed: 17804609]
20. Chien V, Aitken JF, Zhang SP, Buchanan CM, Hickey A, Brittain T, Cooper GJS, Loomes KM. The chaperone proteins HSP70, HSP40/DnaJ and GRP78/BiP suppress misfolding and formation of beta-sheet-containing aggregates by human amylin: a potential role for defective chaperone biology in Type 2 diabetes. Biochem J. 2010; 432:113–121. [PubMed: 20735358]
21. Kienzl E, Puchinger L, Jellinger K, Linert W, Stachelberger H, Jameson RF. The role of transition metals in the pathogenesis of Parkinson's disease. J Neurol Sci. 1995; 134:69–78. [PubMed: 8847547]
22. Bush AI. The metallobiology of Alzheimer's disease. Trends Neurosci. 2003; 26:207–214. [PubMed: 12689772]
23. Rana A, Gnaneswari D, Bansal S, Kundu B. Prion metal interaction: Is prion pathogenesis a cause or a consequence of metal imbalance? Chem-Biol Interact. 2009; 181:282–291. [PubMed: 19660443]
24. Uversky VN, Li J, Fink AL. Metal-triggered structural transformations, aggregation, and fibrillation of human alpha-synuclein - A possible molecular link between Parkinson's disease and heavy metal exposure. J Biol Chem. 2001; 276:44284–44296. [PubMed: 11553618]
25. Drago D, Bolognin S, Zatta P. Role of metal ions in the Aβ oligomerization in Alzheimer's disease and in other neurological disorders. Curr Alzheimer Res. 2008; 5:500–507. [PubMed: 19075576]
26. Ward B, Walker K, Exley C. Copper(II) inhibits the formation of amylin amyloid in vitro. J Inorg Biochem. 2008; 102:371–375. [PubMed: 18022240]

27. Kim BJ, Kim YH, Kim S, Kim JW, Koh JY, Oh SH, Lee MK, Kim KW, Lee MS. Zinc as a paracrine effector in pancreatic islet cell death. Diabetes. 2000; 49:367–372. [PubMed: 10868957]
28. Chang I, Cho N, Koh JY, Lee MS. Pyruvate inhibits zinc-mediated pancreatic islet cell death and diabetes. Diabetologia. 2003; 46:1220–1227. [PubMed: 12898018]
29. Schott-Ohly P, Lgssiar A, Partke HJ, Hassan M, Friesen N, Gleichmann H. Prevention of spontaneous and experimentally induced diabetes in mice with zinc sulfate-enriched drinking water is associated with activation and reduction of NF-kappa B and AP-1 in islets, respectively. Exp Biol Med. 2004; 229:1177–1185.
30. Foster MC, Leapman RD, Li MX, Atwater I. Elemental composition of secretory granules in pancreatic islets of Langerhans. Biophys J. 1993; 64:525–532. [PubMed: 8457676]
31. Faller P. Copper and zinc binding to amyloid-β: coordination, dynamics, aggregation, reactivity and metal-ion transfer. ChemBioChem. 2009; 10:2837–2845. [PubMed: 19877000]
32. Gaggelli E, Bernardi F, Molteni E, Pogni R, Valensin D, Valensin G, Remelli M, Luczkowski M, Kozlowski H. Interaction of the human prion PrP(106–126) sequence with copper(II), manganese(II), and zinc(11): NMR and EPR studies. J Am Chem Soc. 2005; 127:996–1006. [PubMed: 15656638]
33. Jobling MF, Huang XD, Stewart LR, Barnham KJ, Curtain C, Volitakis I, Perugini M, White AR, Cherny RA, Masters CL, Barrow CJ, Collins SJ, Bush AI, Cappai R. Copper and zinc binding modulates the aggregation and neurotoxic properties of the prion peptide PrP106–126. Biochemistry. 2001; 40:8073–8084. [PubMed: 11434776]
34. Taylor CG. Zinc, the pancreas, and diabetes: Insights from rodent studies and future directions. Biometals. 2005; 18:305–312. [PubMed: 16158221]
35. Chausmer AB. Zinc, insulin and diabetes. J Am Coll Nutr. 1998; 17:109–115. [PubMed: 9550453]
36. Zhou HR, Zhang T, Harmon JS, Bryan J, Robertson RP. Zinc, not insulin, regulates the rat alpha-cell response to hypoglycemia in vivo. Diabetes. 2007; 56:1107–1112. [PubMed: 17317764]
37. Brender JR, Hartman K, Nanga RPR, Popovych N, Bea RD, Vivekanandan S, Marsh ENG, Ramamoorthy A. Role of zinc in human islet amyloid polypeptide aggregation. J Am Chem Soc. 2010; 132:8973–8983. [PubMed: 20536124]
38. Falconer RJ, Penkova A, Jelesarov I, Collins BM. Survey of the year 2008: applications of isothermal titration calorimetry. J Mol Recognit. 2010; 23:395–413. [PubMed: 20213668]
39. Brender JR, Hartman K, Reid KR, Kennedy RT, Ramamoorthy A. A Single Mutation in the Nonamyloidogenic Region of Islet Amyloid Polypeptide Greatly Reduces Toxicity. Biochemistry. 2008; 47:12680–12688. [PubMed: 18989933]
40. Nanga RPR, Brender JR, Xu JD, Veglia G, Ramamoorthy A. Structures of rat and human islet amyloid polypeptide IAPP(1–19) in micelles by NMR spectroscopy. Biochemistry. 2008; 47:12689–12697. [PubMed: 18989932]
41. Brender JR, Lee EL, Cavitt MA, Gafni A, Steel DG, Ramamoorthy A. Amyloid fiber formation and membrane disruption are separate processes localized in two distinct regions of IAPP, the type-2-diabetes-related peptide. J Am Chem Soc. 2008; 130:6424–6429. [PubMed: 18444645]
42. Engel MFM, Yigittop H, Elgersma RC, Rijkers DTS, Liskamp RMJ, de Kruijff B, Hoppener JWM, Killian JA. Islet amyloid polypelptide inserts into phospholipid monolayers as monomer. J Mol Biol. 2006; 356:783–789. [PubMed: 16403520]
43. Andrews ME, Inayathullah NM, Jayakumar R, Malar EJP. Conformational polymorphism and cellular toxicity of IAPP and beta AP domains. J Struct Biol. 2009; 166:116–125. [PubMed: 19374013]
44. Higham CE, Jaikaran E, Fraser PE, Gross M, Clark A. Preparation of synthetic human islet amyloid polypeptide (IAPP) in a stable conformation to enable study of conversion to amyloid-like fibrils. FEBS Lett. 2000; 470:55–60. [PubMed: 10722845]
45. Padrick SB, Miranker AD. Islet amyloid: Phase partitioning and secondary nucleation are central to the mechanism of fibrillogenesis. Biochemistry. 2002; 41:4694–4703. [PubMed: 11926832]
46. Yonemoto IT, Kroon GJ, Dyson HJ, Balch WE, Kelly JW. Amylin proprotein processing generates progressively more amyloidogenic peptides that initially sample the helical state. Biochemistry. 2008; 47:9900–9910. [PubMed: 18710262]

47. Mishra R, Geyer M, Winter R. NMR spectroscopic investigation of early events in IAPP amyloid fibril formation. ChemBioChem. 2009; 10:1769–72. [PubMed: 19575373]
48. Wiltzius JJ, Sievers SA, Sawaya MR, Eisenberg D. Atomic structures of IAPP (amylin) fusions suggest a mechanism for fibrillation and the role of insulin in the process. Protein Sci. 2009; 18:1521–30. [PubMed: 19475663]
49. Mazor Y, Gilead S, Benhar I, Gazit E. Identification and characterization of a novel molecular-recognition and self-assembly domain within the islet amyloid polypeptide. J Mol Biol. 2002; 322:1013–1024. [PubMed: 12367525]
50. Williamson JA, Miranker AD. Direct detection of transient alpha-helical states in islet amyloid polypeptide. Protein Sci. 2007; 16:110–117. [PubMed: 17123962]
51. Kajava AV, Aebi U, Steven AC. The parallel superpleated beta-structure as a model for amyloid fibrils of human amylin. J Mol Biol. 2005; 348:247–252. [PubMed: 15811365]
52. Abedini A, Raleigh DP. The role of His-18 in amyloid formation by human islet amyloid polypeptide. Biochemistry. 2005; 44:16284–16291. [PubMed: 16331989]
53. Charge SBP, Dekoning EJP, Clark A. Effect of pH and insulin on fibrillogenesis of islet amyloid polypeptide in-vitro. Biochemistry. 1995; 34:14588–14593. [PubMed: 7578065]
54. Aruga R. Thermodynamics of complex-formation of 1-methylimidazole with cobalt(II), nickel(II), copper(II) and zinc(II) cations in aqueous-solution. Transition Met Chem (London). 1983; 8:56–58.
55. Chakravorty A, Cotton FA. Stability constants and structures of some metal complexes with imidazole derivatives. J Phys Chem. 1963; 67:2878–2879.
56. Auld DS. The ins and outs of biological zinc sites. Biometals. 2009; 22:141–148. [PubMed: 19140015]
57. Vallee BL, Auld DS. Zinc coordination, function, and structure of zinc enzymes and other proteins. Biochemistry. 1990; 29:5647–5659. [PubMed: 2200508]
58. Reddy AS, Wang L, Singh S, Ling YL, Buchanan L, Zanni MT, Skinner JL, de Pablo JJ. Stable and metastable states of human amylin in solution. Biophys J. 2010; 99:2208–2216. [PubMed: 20923655]
59. Dupuis NF, Wu C, Shea JE, Bowers MT. Human islet amyloid polypeptide monomers form ordered beta-hairpins: a possible direct amyloidogenic Precursor. J Am Chem Soc. 2009; 131:18283–18292. [PubMed: 19950949]
60. Knight JD, Hebda JA, Miranker AD. Conserved and cooperative assembly of membrane-bound alpha-helical states of islet amyloid polypeptide. Biochemistry. 2006; 45:9496–9508. [PubMed: 16878984]
61. Yonemoto IT, Kroon GJA, Dyson HJ, Balch WE, Kelly JW. Amylin proprotein processing generates progressively more amyloidogenic peptides that initially sample the helical state. Biochemistry. 2008; 47:9900–9910. [PubMed: 18710262]
62. Saraogi I, Hebda JA, Becerril J, Estroff LA, Miranker AD, Hamilton AD. Synthetic α-helix mimetics as agonists and antagonists of islet amyloid polypeptide aggregation. Angew Chem-Int Ed. 2010; 49:736–739.
63. Williamson JA, Loria JP, Miranker AD. Helix Stabilization Precedes Aqueous and Bilayer-Catalyzed Fiber Formation in Islet Amyloid Polypeptide. J Mol Biol. 2009; 393:383–396. [PubMed: 19647750]
64. Wiltzius JJW, Sievers SA, Sawaya MR, Eisenberg D. Atomic structures of IAPP (amylin) fusions suggest a mechanism for fibrillation and the role of insulin in the process. Protein Sci. 2009; 18:1521–1530. [PubMed: 19475663]
65. Patil SM, Xu SH, Sheftic SR, Alexandrescu AT. Dynamic α-helix structure of micelle-bound human amylin. J Biol Chem. 2009; 284:11982–11991. [PubMed: 19244249]
66. Cort JR, Liu Z, Lee GM, Huggins KN, Janes S, Prickett K, Andersen NH. Solution state structures of human pancreatic amylin and pramlintide. Protein Eng Des Sel. 2009; 22:497–513. [PubMed: 19596697]
67. Kirkitadze MD, Condron MM, Teplow DB. Identification and characterization of key kinetic intermediates in amyloid beta-protein fibrillogenesis. J Mol Biol. 2001; 312:1103–1119. [PubMed: 11580253]

68. Fezoui Y, Teplow DB. Kinetic studies of amyloid beta-protein fibril assembly - Differential effects of α-helix stabilization. J Biol Chem. 2002; 277:36948–36954. [PubMed: 12149256]

69. Maret W, Li Y. Coordination dynamics of zinc in proteins. Chem Rev (Washington, DC, U S). 2009; 109:4682–4707.

70. Goldfarb AR, Saidel LJ, Mosovich E. The Ultraviolet Absorption Spectra of Proteins. J Biol Chem. 1951; 193:397–404. [PubMed: 14907727]

71. Scopes RK. Measurement of Protein by Spectrophotometry at 205-nm. Anal Biochem. 1974; 59:277–282. [PubMed: 4407487]

72. Hernandez H, Robinson CV. Determining the stoichiometry and interactions of macromolecular assemblies from mass spectrometry. Nat Protoc. 2007; 2:715–726. [PubMed: 17406634]

73. Schanda P, Forge V, Brutscher B. Protein folding and unfolding studied at atomic resolution by fast two-dimensional NMR spectroscopy. Proc Natl Acad Sci U S A. 2007; 104:11257–11262. [PubMed: 17592113]

74. Goddard, TD.; Kneller, DG. SPARKY 3. University of California; San Francisco: 1999.

Research Highlights

- IAPP has micro and millimolar affinity binding sites for zinc.
- hIAPP fibers display a decreased affinity for zinc compared to the monomeric form.
- hIAPP binds to zinc as a hexamer by minimizing unfavorable steric interactions.
- The displacement of zinc precedes the formation of mature fiber.
- Zinc inhibits the formation of the hIAPP dimer and mature fiber while promoting oligomers.

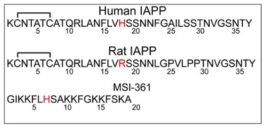

Figure 1.

Amino acid sequences of the peptides used. All unlabelled peptides are amidated and contain oxidized cysteines. The imidazole of His 18 can bind to zinc and the substitution of arginine for histidine in rat IAPP removes a potential zinc binding site.

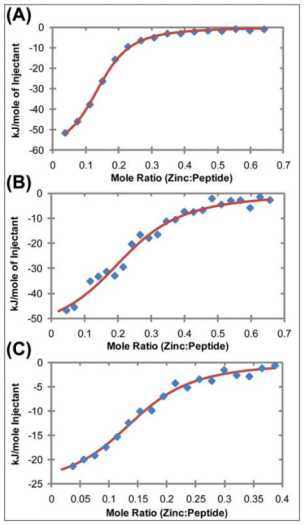

Figure 2.

Heat evolved from the titration of $ZnCl_2$ into $hIAPP_{1–19}$ with 100 mM Tris buffer and (A) 100 μM NaCl, (B) 100 μM NaCl with 30%TFE, and with (C) 100 mM NaCl. The data was fit to a single binding site model and the apparent thermodynamic parameters can be found in Table 1. All ITC experiments were conducted at pH 7.3 and 25°C

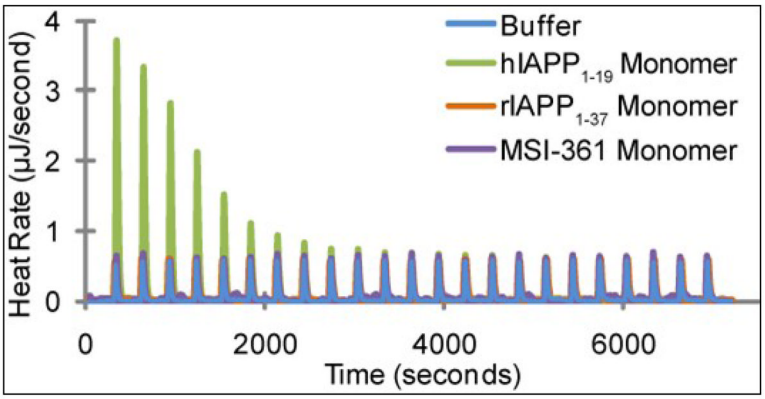

Figure 3.

Heat evolved from the titration of $ZnCl_2$ into buffer (100 mM Tris buffer and 100μM NaCl), $hIAPP_{1–19}$, and MSI-361 under identical conditions. The heat evolved from the interaction between MSI-361 and zinc is comparable in magnitude to the control, and significantly less than the interaction between $hIAPP_{1–19}$ and zinc. Since both peptides are 19 residues long and contain one histidine, the results indicate that the observed interaction between hIAPP and zinc are sequence specific.

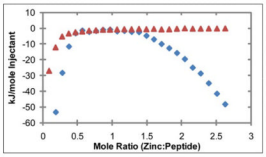

Figure 4.

Heat evolved from the titration of $ZnCl_2$ into $hIAPP_{1–19}$ at pH 7.3 and 25°C, as measured by ITC. In solution with 100 mM Tris buffer and 100 μM NaCl (▲), zinc has one apparent binding site at sub- stoichiometric ratios of 0.136 zinc to 1 $hIAPP_{1–19}$. In the presence of 30% TFE (◆) the peptide adopts an α-helical conformation, causing a shift in the apparent binding stoichiometry of the primary binding site to 0.24 zinc to 1 $hIAPP_{1–19}$ and the addition of an endothermic process at higher concentrations of zinc.

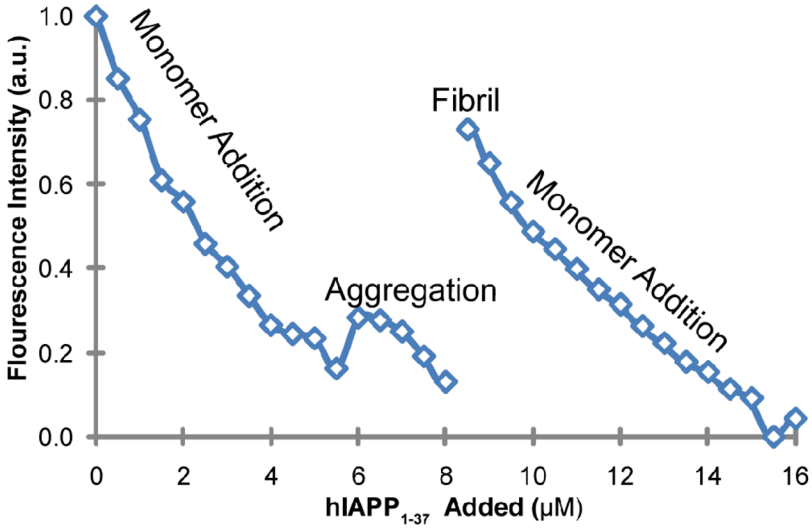

Figure 5.

Addition of $hIAPP_{1–37}$ to 2.5 μM of the fluorescence zinc sensor, FluoZin-1, and 2.5 μM zinc. A decrease in fluorescence intensity corresponds to zinc being displaced from the zinc sensor and binding to the peptide. The solution was initially maintained at 4 °C to prevent aggregation. At the 6 μM titration point the temperature was raised to 25 °C. The peptide was allowed to stand at the 8 μM titration point until aggregation became evident by the turbidity of the solution. The increase in fluorescence intensity at 8 μM indicates the zinc is being displaced from the peptide by fibrillization. The decrease in fluorescence after addition of fresh peptide confirms the sensor is still binding zinc after fibrillization.

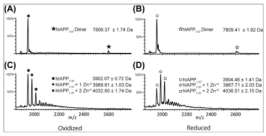

Figure 6.

ESI-MS spectra of oxidized (A, C) and reduced (B, D) $hIAPP_{1–37}$ in absence (A, B) of zinc and presence (C, D) of 1 mM zinc. In the absence of zinc, a +2 oxidized monomer peak is observed at 1952 m/z (A) and a +2 reduced monomer peak is observed at 1954 m/z (B). A minor +3 dimer peak is also observed at 2604 m/z for oxidized IAPP and 2605 m/z for reduced IAPP. The addition of zinc to oxidized IAPP (C) reveals +2 monomer peaks at 1984 m/z and 2017 m/z, corresponding to monomers bound to 1 and 2 zinc ions respectively. Similar +2 monomer peaks were observed at 1985 m/z and 2018 m/z with the addition of zinc to the reduced peptide (D). Compared to oxidized hIAPP, a greater proportion of reduced hIAPP is bound to 1 and 2 zinc ions, indicating the presence of non-native interactions with cysteine after reduction of the disulfide bond. No peaks were observed near 2604 m/z with the addition of zinc.

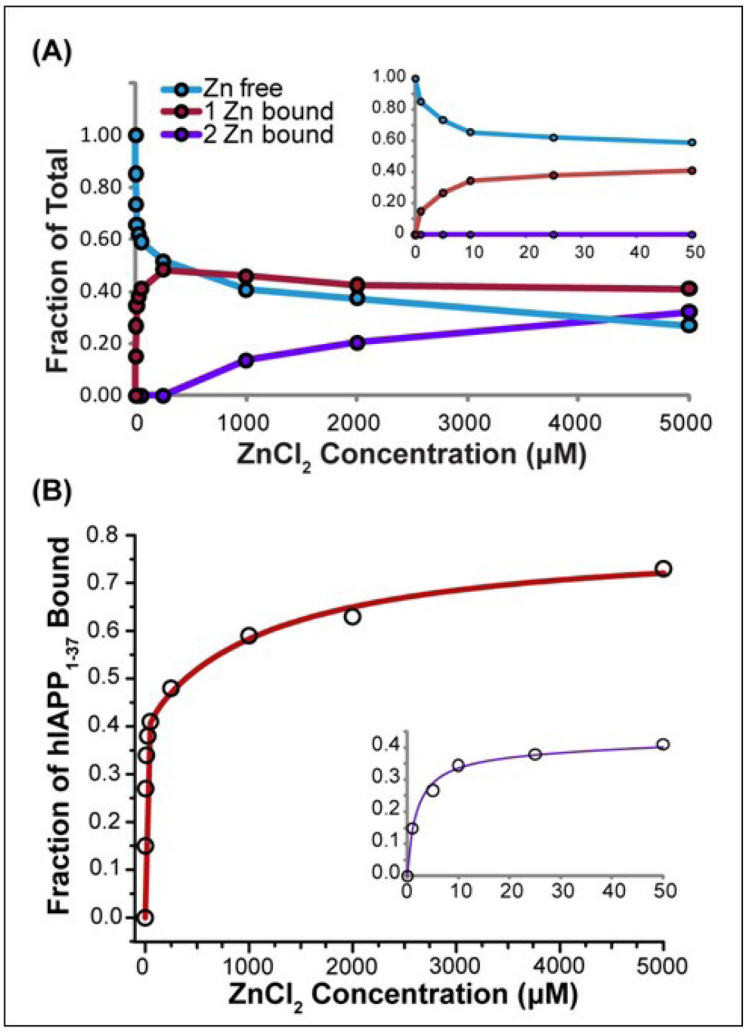

Figure 7.

(A) Concentration dependence of zinc binding of 10 μM $hIAPP_{1–37}$ by ESI-MS. The first binding site is saturated at 10 μM $ZnCl_2$, while a second binding site becomes evident at 1000 μM $ZnCl_2$. **(B)** Comparison of experimental values to a fit of the data according to a two site independent binding model. A close-up of the low zinc concentration values is shown in the inset. K_d values from the fit were calculated to be 2 ± 0.3 μM and 1200 ± 300 μM.

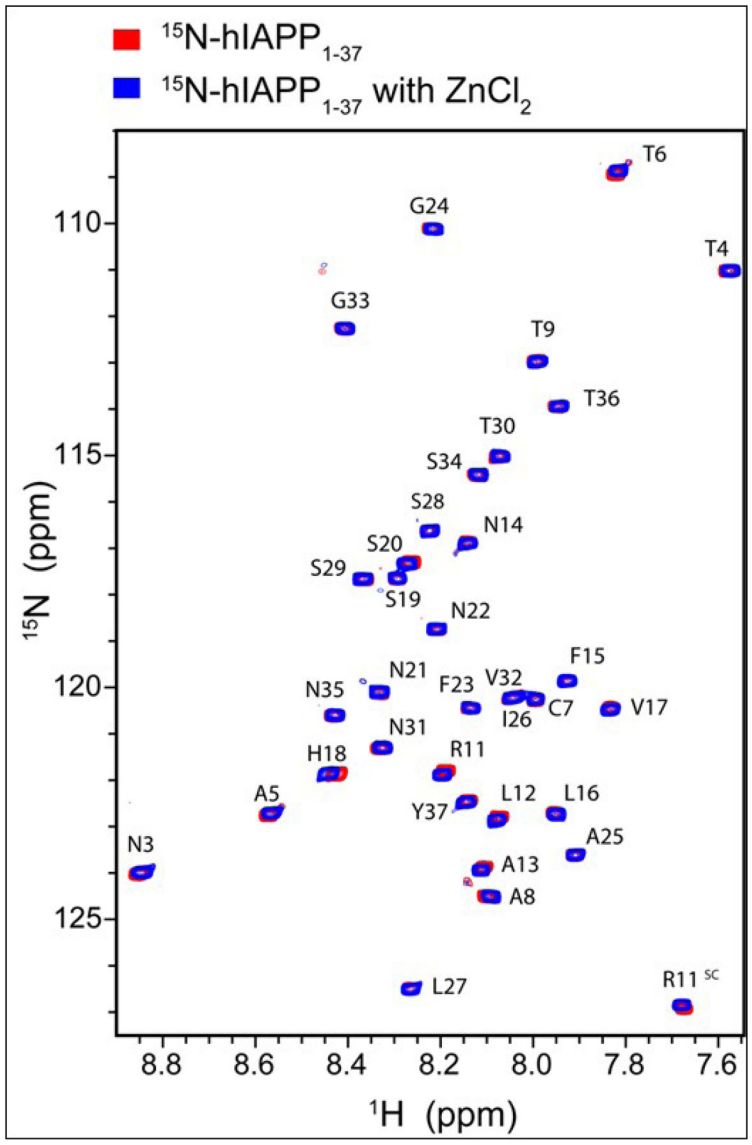

Figure 8.

Overlay of SOFAST-HMQC spectra of ^{15}N-hIAPP$_{1–37}$ in the presence (blue) and absence (red) of zinc chloride at pH 5. The greatest chemical shift occurs at His 18; however, Thr 6, Arg 11, and Leu 12 display significant chemical shifts as well.

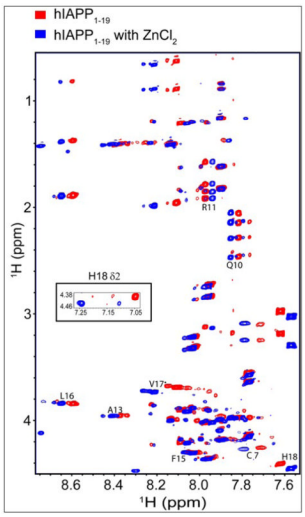

Figure 9.

Overlay of the 2D ^{1}H-^{1}H TOCSY spectra of hIAPP$_{1–19}$ in solution and a select region of the NOESY spectra in the absence (red) and presence (blue) of 10 mM $ZnCl_2$. Addition of zinc causes downfield shifts for the H_N proton residues of Cys 7, Glu 10, Ala 13, Leu 16, Val 17 and upfield shifts for residues Arg 11 and His 18. A significant up-field shift of 0.2 ppm for the $H_{\delta 2}$ proton of His 18 is observed upon the addition of zinc (shown in the NOESY strip).

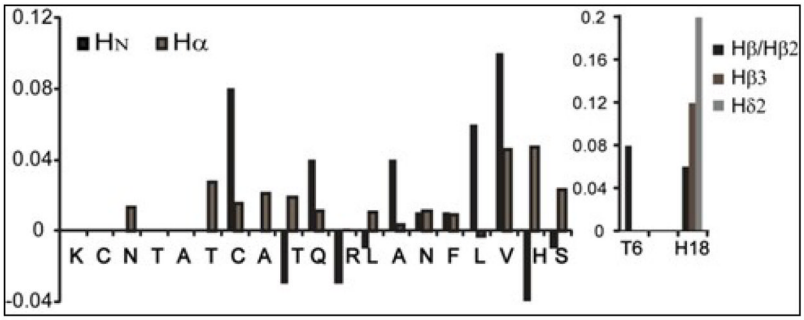

Figure 10.

Changes in H_α and H_N chemical shifts of $hIAPP_{1–19}$ upon binding to zinc. Also shown are side chain chemical shift differences of Thr 6 (H_β) and His 18 ($H_{\beta2/3}$ and $H_{\delta2}$). Noticeable differences are localized at Thr 6, Cys 7, Leu 16, Val 17 and His 18.

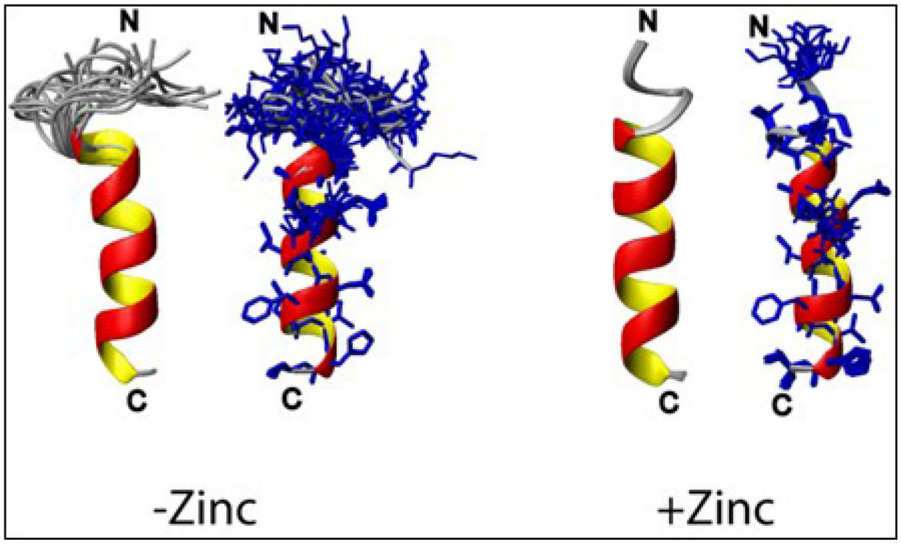

Figure 11.

High-resolution NMR structures of $hIAPP_{1–19}$ in the absence (left) and in the presence (right) of 10 mM $ZnCl_2$. Zinc binding induces ordering of the secondary structure at the N-terminus. In the absence of zinc, Gln 10, Asn 14, His 18 are oriented in same plane whereas Asn 14 and His 18 are in the same plane with the His 18 ring flipped horizontally while Gln 10 is moved closer to the N-terminus.

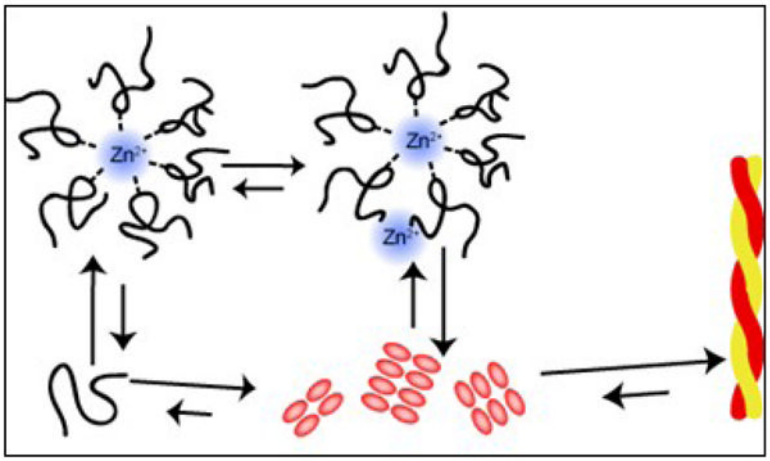

Figure 12.

Diagram of the fibrillization pathway in the presence of zinc, not drawn to scale. In the presence of zinc, the formation of off-pathway hexameric species is stabilized while the formation of dimers is inhibited. Since zinc does not appreciably interact with the mature fibril, the dissociation of zinc poses a large thermodynamic barrier for the formation of mature fiber.

Table 1

Apparent thermodynamic parameters obtained from ITC titration of $ZnCl_2$ into peptide.

Peptide and buffer	K_d(μM)	ΔG (kJ/mole)	ΔH (kJ/mol)	ΔS (J/mol)	n (zinc:peptide)
hIAPP 1–19 in low ionic strength buffer (100μM NaCl)	1.12 ± 0.2	−33.9 ± 0.3	−61.9 ± 2.4	−93.8 ± 8.1	0.136 ± 0.004
hIAPP 1–19 in low ionic strength buffer (100μM NaCl) with 30% TFE	2.26 ± 1.6	−32.2 ± 1.4	−56.1 ± 8.3	−80.2 ± 28.1	0.241 ± 0.023
hIAPP 1–19 in high ionic strength buffer (100 mMNaCl)	1.23 ± 0.5	−33.7 ± 0.8	−25.6 ± 2.2	+27.2 ± 7.9	0.151 ±0.009